# Fabrication of Cobalt-Doped Lignin Base Carbon Nanotubes Composite Material for Energy Storage Applications

[1]Zaib Ullah Khan, [1,2]Jinghua Jiang*, [3]Zahid Ullah, [4]Muhammad Yasir Ali Khan and [5]Asifa Kusar
[1]*College of Mechanics and Materials, Hohai University, Nanjing 211100, China.*
[2]*Suqian Institute of Hohai University, Suqian 223800, China.*
[3]*Department of Material Science and Engineering, University of New South Wales, Sydney, Australia.*
[4]*College of Water Conservancy and Hydropower, Hohai University, Nanjing 211100, China.*
[5]*Pakistan Institute of Engineering and Applied Sciences Nilore, Islamabad 45650, Pakistan.*
jinghua-jiang@hhu.edu.cn*

(Received on 2nd September 2024, accepted in revised form 23rd May 2025)

**Summary:** The development of high-performance, sustainable, and economical electrodes with superior capacity and cyclic stability is crucial for the advancement of energy storage devices. Carbon nanotubes (CNTs) has garnered considerable interest as a potential electrode material for energy storage applications, owing to its high capacity, natural abundance, cost-effectiveness, and eco-friendliness. In the present study, lignin was combined with CNTs to synthesize a Co-CNTs/lignin composite electrode material via hydrothermal method, for enhance energy storage performance. The structure and surface morphology of the synthesized Co-CNTs/lignin composite is characterized by X-ray diffraction (XRD), RAMAN spectroscopy, X-ray Photoelectron Spectroscopy (XPS), scanning electron microscopy (SEM), and Brunauer-Emmett-Teller (BET). The thermal stability of the composite sample was also studied by thermogravimetric analysis (TGA). The Co-CNTs/lignin composite exhibit enhanced electrochemical kinetics and electrical conductivity compared to pristine Co-CNTs and Co-lignin. The Co-CNTs/lignin composite material has shown remarkable electrochemical performance, it exhibits high specific capacitance, an energy density, and a power density at a low current density. The composite material showed outstanding electrochemical stability, maintaining 98% of its original capacitance and exhibiting an impressive coulombic efficiency of 81% after 1000 charge-discharge cycles at a current density of 5 A $g^{-1}$. The obtained data indicated that the composite materials exhibit superior performance in energy storage devices.

**Keywords:** Lignin, Carbon Nanotubes, Energy Storage, Composite material, Electrochemistry.

## Introduction

As the demand for resources increases and fossil fuels deplete rapidly, people are exploring renewable energy sources and innovative energy storage methods to address the energy problem. Recently, there has been an increasing demand to discover additional sources of renewable energy that are readily available and have positive environmental impacts. A widely held belief is that harnessing plant energy is the most efficient and ecologically friendly method to substitute fossil fuels. Globally, generate a staggering 60 billion tons of plant material annually, with lignin serving as a prominent constituent. Therefore, some have viewed the use of biofuel, specifically the combustion of lignin, as a viable replacement for certain fossil fuels. However, conventional methods find it more challenging to convert lignin into fossil fuels due to its intricate chemical composition and diverse molecular weights [1].

Composite electrode materials, such as CNTs [2], carbon fiber paper [3], carbon nanofoams [4], graphene [5] or templated mesoporous carbon [6], organize nanostructured metal parts on a conductive base with a lot of specific surface area. They are the optimal and efficient means to enhance the performance of electricity, and they can serve as an electrode in both secondary batteries and supercapacitors. Optimization is critical for the second application because electrochemical reactions occur at or near the surface. CNTs are exceptionally well-suited as templates, owing to their high aspect ratio and straightforward production process. They can be readily synthesized from plentiful, cost-effective, and non-toxic carbon sources, making them an attractive choice for researchers seeking a reliable and sustainable material for their work. However, in practical applications, it is crucial to securely bond CNTs to metals, either by adhering them to the metal surfaces or by connecting them to the metal ends [7].

Additionally, lignin possesses numerous favorable attributes, including resistance to oxidation, spontaneous decomposition, high calorific value, and

***To whom all correspondence should be addressed.**

stability under elevated temperatures [8]. Because of these characteristics, lignin plays an important role in everyday applications and materials. The pulp and paper sector extensively utilizes lignin as a fuel source, capitalizing on its substantial calorific value to generate thermal and electrical energy. The high energy content of lignin makes it an indispensable resource for the industry, enabling the production of heat and power while minimizing dependence on external energy supplies. Polymer research has utilized lignin as a versatile component, serving both functional and structural roles in the synthesis of polymer compounds [9, 10]. Lignin has a multitude of reactive functional groups, which makes it a suitable raw material for manufacturing several kinds of detergents [11]. Although lignin has found numerous applications, its extensive use in high-value applications remains unexplored [12]. Therefore, conducting further research on optimizing the utilization of lignin to maximize its significant economic worth is imperative in order to fully exploit biomass resources [13]. Tao *et al*. [14] discovered a creative way to transform walnut shells into flexible, self-supporting carbon nanofiber screens. They intentionally designed these membranes for use in advanced lithium-ion batteries, showcasing a promising application for sustainable materials in high-performance energy storage. Xu *et al*. [15] performed a research to investigate the heat stability of alkaline lignin , examining the transformations of oxygen-containing functional groups at a temperature of 290 °C. Their research revealed three discrete phases in the thermal decomposition of alkaline lignin, contributing to a deeper understanding of its thermal behaviour and potential applications. You *et al*. [16] fabricated lignin fibers derived from cedar wood to fabricate electrodes for double-layer capacitors. Zhang *et al*. [17] successfully synthesized a novel nanocarbon network by combining lignin and cellulose acetate, achieving a surface area of 540.95 $m^2$ $g^{-1}$. The researchers investigated the suitability of this compound as an anode material for sodium-ion battery, demonstrating its potential for enhancing energy storage capabilities. Park *et al*. [18] utilize lignin to create a hydrogel solution and nanofiber electrodes that are self-sufficient. These data demonstrate the robustness of their strength, their exceptional ability to conduct ions, and the interconnectedness of their open structure, enabling them to store a significant amount of electrical charge.

In this work, we successfully synthesized Co-CNTs/lignin composite material by simple hydrothermal method, which demonstrates outstanding electrochemical performance for energy storage applications. This study introduces a combination of carbon nanotubes, cobalt oxides with lignin, which improves the materials conductivity, electrochemical performance, and structural stability. The large surface area of 703.6 $m^2$ $g^{-1}$, a pore volume of 0.39 $cm^3$ $g^{-1}$, and pore size is concentrated with 1.5–3.5 nm pore diameter, which facilitate electrolyte penetration, ion diffusion charge mobility. Overall, the high-performance, long-term stability, high-efficiency electrochemical performance establish a platform for the development of cost-effective, scalable, and high-performance electrodes for energy storage applications.

## Experimental

### *Materials and Methods*

### *Materials*

We obtained the necessary chemicals for our research from various suppliers. Specifically, Huatai Group Co., Ltd. in Dongying, China provided us with a selection of essential chemicals, including sulphuric acid, nitric acid, membrane filters, hydrazine hydrate, and lignin, which were essential for our experiments. Aqueous solutions prepared from these compounds exhibited a pH of approximately 3. We also obtained other chemicals from Aladdin, including p-Phenylenediamine, cobalt (ll) acetate tetrahydrate, melamine, potassium hydroxide, Nafion solution, and ethanol. Additionally, we got the Pt/C catalyst, which contains 20% platinum, from Johnson Matthey Corp. We used all these reagents without any further purification.

### *Lignin isolation from black liquor samples*

In order to separate lignin, combined 125 ml of 1 M sulfuric acid with 20 ml of black liquor at room temperature. Next, meticulously collected the biopolymer by vacuum filtration using a polytetrafluoroethylene (PTFE) sheet. Then washed the lignin with distilled water at least five times. Subsequently, the material was subjected to thermal curing at 80 °C in a closed environment without ventilation. The concentration of lignin in each unit of black liquor was quantified and expressed in grams per liter ($g\ L^{-1}$).

### *CNTs Synthesis*

Through the implementation of the chemical vapor deposition technique, we successfully produced vertically aligned carbon nanotubes, demonstrating a high degree of control and precision in their growth and alignment. Toluene was employed as the carbon

precursor, while ferrocene served as the catalyst [19]. High-frequency electromagnetic waves were employed to cure the toluene solution containing 3% ferrocene. The experiment was conducted in a horizontally-oriented oven equipped with three distinct types of heating sources. Maintained a constant temperature of 760 °C in the argon atmosphere throughout the duration of the interaction. Combine 0.5 g of CNTs with 187.5 ml of sulphuric acid and 62.5 ml of nitric acid in a 500 ml flask to create the mixture. Following the mixing procedure, treat the mixture to ultrasonic agitation at a precisely maintained temperature of 50 °C for 20 hours, thereby ensuring thorough dispersion and optimal reaction conditions. Additionally, 1000 g $L^{-1}$ distilled water were introduced to dilute the chemical. After completing the previous step, the PTFE membrane filters were placed onto a fritted-glass tube and pressure was exerted. Subsequently, the specimens were allowed to desiccate for the duration of one night at a temperature of 110 °C.

*Synthesis of Co-CNTs/lignin*

Successfully prepared a homogeneous solution by subjecting the mixture to ultrasonic waves for two hours and introducing 0.06 g of CNTs into 40 mL of deionized water. Next, introduced 0.05 g of cobalt (II) acetate tetrahydrate and 0.5 g of p-phenylenediamine into the suspension, thoroughly blending them for four hours at room temperature. Subsequently, the suspension was moved to a Teflon-lined stainless-steel autoclave, where it undertook a high-temperature process at 180 °C for 12 hours. After subjecting the sample to heat treatment, the resultant black-purple substance was separated using centrifugation and then washed extensively with deionised water to eliminate any impurities. Finally, heated the power in a nitrogen ($N_2$) environment at 850 °C for two hours, at a rate of 10 °C per minute and collect Co-CNTs/lignin. To facilitate comparison, we also fabricated Co-lignin and Co-CNTs using the same procedure under control system.

*Fabrication of Co-CNT/lignin-GCE electrode*

The probe was constructed using a glassy carbon electrode (GCE), and use an alumina slurry to purify the surface of GCE. In order to modify the GCE surface, a solution was prepared by mixing 0.5-1 mg of Co-CNTs/lignin composite with 1 mL of ethanol, and then subjecting it to sonication for 1 hour, to get homogenous solution. The same procedure was repeated for the remaining two synthesized materials. The solution was then deposited onto the pristine GCE surface, which had a diameter of 3 mm, and left to dry at room temperature for 24 hours. After the successful modification of the GCE, the resulting electrode was designated as Co-CNTs/lignin-GCE and subsequently employed for electrochemical analyses. **Fig. 1** shows a schematic illustration of Co-CNTs/lignin synthesis, modification of the GCE surface, as well as electrochemical testing of the fabricated electrode. Same method use for Co-CNTs and Co-lignin to modify the surface of GCE.

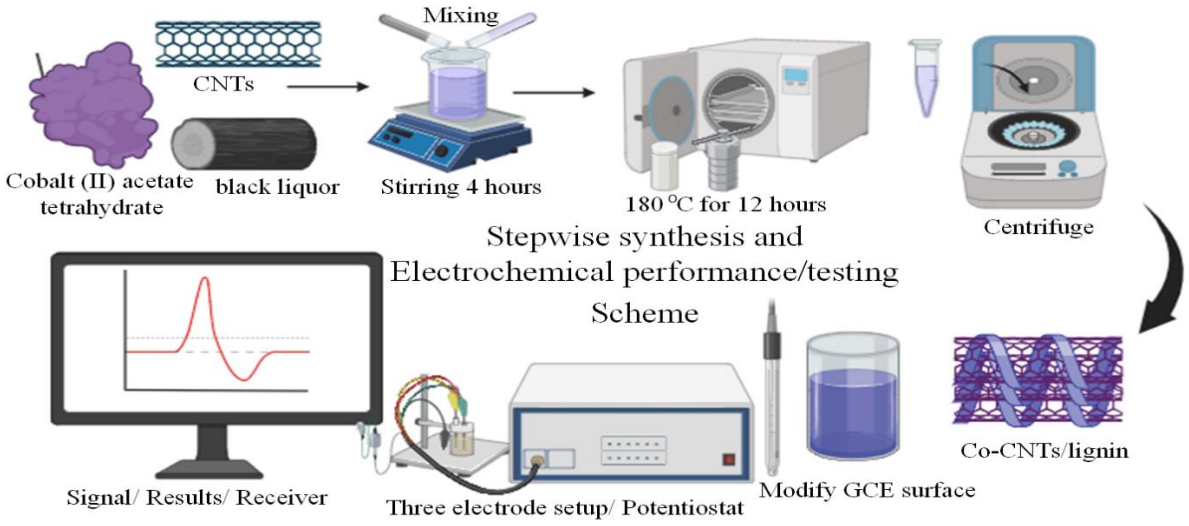


Fig. 1: Systematic illustration of Co-CNTs/lignin synthesis, modifying the surface of GCE and electrochemical testing.

*Characterization*

The variety of methods to thoroughly analyzed the materials we synthesized. The Rigaku Ultima IV diffractometer was used to conduct X-ray diffraction tests. The study was carried out using copper radiation with a wavelength of 1.541 nm, a voltage of 40 kV, and a current of 40 mA, and the scanning rate was 10–80 degrees. The micro-morphology was studied using scanning electron microscopy on a Tescan Vega Compact at 20 kV. The Raman spectroscopy investigation was carried out using an InVia Raman Microscope from RENISHAW UK. The excitation laser had a wavelength of 514 nm. The exposure time was set at 10 seconds, the grating density at 1800 lines per millimetre, and the laser intensity was set to 100%. Thermal stability was evaluated using thermogravimetric analysis on a Mettler Toledo analyzer under a nitrogen atmosphere, with a heating rate of 10 °C per minute. Surface chemical composition was examined via X-ray photoelectron spectroscopy using a Thermo Scientific Escalab-250Xi system with Al-Kα as the excitation source. Textural properties, including specific surface area and pore volume, were determined using the Brunauer–Emmett–Teller method with nitrogen adsorption–desorption measurements on a Micromeritics ASAP 2020 system. For electrochemical measurements, we utilized a Gamry Potentiostat (model 1010E, serial number 23045).

*Electrochemical Measurements*

A three electrodes system was utilized to investigate the electrochemical properties of the synthesized samples in 6 M KOH electrolyte. The counter electrode was a platinum (Pt) wire, the reference electrode was Ag/AgCl, and the working electrode was a modify-GCE. The following equation was used to analyse the galvanostatic charge-discharge patterns and calculate the specific capacitance:

$$C_s = \frac{I\Delta t}{m\Delta V} \quad (1)$$

The equation allows us to determine the specific capacitance ($C_s$) by taking into account variables such as the discharge current (I), discharge duration (Δt), mass of active material (m), and discharge voltage (ΔV). In addition, to used supplementary equations to calculate the energy density ($E_g$) in Wh $kg^{-1}$ and power density ($P_w$) in W $kg^{-1}$, which are essential metrics for assessing the efficiency of our synthesized materials:

$$E_g = \frac{C_s \Delta V^2}{2\times 3.6} \quad (2)$$

$$P_w = \frac{E}{\Delta t} \times 3600 \quad (3)$$

where the symbol '$C_s$' represents the specific capacitance measured in F $g^{-1}$, 'Δt' represents the discharge duration measured in seconds (s), and 'ΔV' represents the discharge voltage measured in volts (V) [20].

**Results and Discussion**

*Structural Characterizations*

Fig (a-d) shows the SEM Images at different magnifications of the synthesized CNTs and Co-CNTs/lignin. Images (a, b) represent pure CNTs, showing a smooth, tubular, and entangled network structure with uniform diameters. The nanotubes appear relatively clean and free of impurities, which is typical for CNTs synthesized without metal doping. The particle appears to be consistent with high-aspect-ratio CNTs useful for conductive frameworks. Images (c, d) show Co-CNTs/lignin composites, where the CNT network is decorated with spherical cobalt nanoparticles and embedded in a lignin matrix. These particles are more densely distributed, and the composite appears rougher and more compact than the pristine CNTs. The Co nanoparticle size ranges from ~100 to 125 nm, forming uniformly dispersed clusters, suggesting effective doping and interaction with lignin. Co-CNTs/lignin composites provide higher roughness, redox-active sites, and stability enhanced electrochemical behavior. This hybrid morphology is ideal for next-generation energy storage devices, particularly supercapacitors, due to improved charge transport, ion diffusion, and mechanical stability.

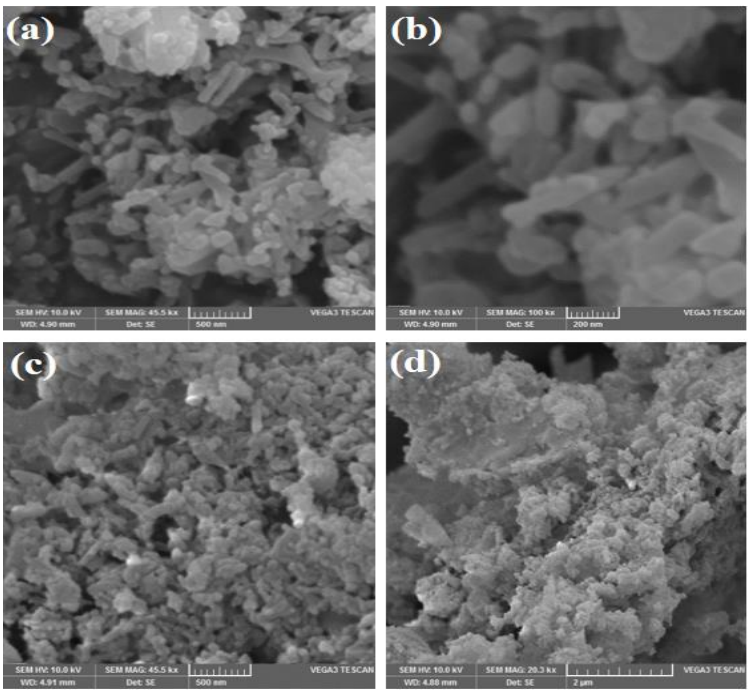


Fig. 2: (a, b) SEM images of the CNTs, and (c, d) Co-CNTs/lignin electrode material at different magnifications, offering a comprehensive visual representation of the synthesized material morphology.

Fig. 3(a) show the X-ray diffraction patterns of the three samples that exhibit distinct variations attributes in their crystalline and compositional structures. This indicates that each sample possesses a unique crystal structure and composition, likely resulting from their specific synthesis conditions and inherent material properties. The curve of Co-CNTs exhibit a broad peaks which indicates the amorphous nature of the sample with notable peaks of 25°, 43°, and 53° [21], corresponding to the plan (002), (100) and (004) [22] of carbon nanotube respectively [23] and the sharp peaks of the Co-lignin curve indicate the formation of crystalline cobalt structure with ligand [24]. The Co-CNTs/lignin sample shows the highest crystalline structure with sharp and intense peak evident the successful integration of cobalt and carbon nanotube with ligands to form composite material [25]. Overall structure of XRD analysis display the amorphous to crystalline phase upon combination of carbon nanotube, cobalt and ligands [26].

The Raman spectroscopy was employed to investigate the degree of graphitization, structural defects, and interaction between Co, CNTs, and lignin in the composite, as shown in Fig. 3(b). The D and G bands provided insights into the disorder and graphitic nature of the carbon matrix, revealing that the Co-CNTs/lignin composite exhibited a higher $I_D/I_G$ ratio compared to pristine Co- CNTs, Co-lignin samples, indicating increased defect sites beneficial for electrochemical activity. Introduction of $sp^3$ hybridized carbon atoms leads to molecular instability, which manifests as the D band at 1352 $cm^{-1}$ [27]. The G band, which occurs at a frequency of 1597 $cm^{-1}$ [28] indicates the existence of carbon domains formed by $sp^2$ hybridization. The recently produced CNTs displayed a highly structured arrangement with a D/G ratio of around 0.83 [29]. After being treated with acid, the CNTs showed a lot of different functional groups, like oxygen, and were partially unzipped, which made them more wavy and disorganized [30]. The oxidation and reduction steps likely led to partial carbon loss through the formation of oxygen-containing functional groups and subsequent removal of labile carbon atoms, as reported in previous studies involving CNT or biomass-derived carbon modification [31]. The D/G ratio of the Co-CNTs/lignin composite subsequently achieved a value of 0.85 [32], and Table 1 highlighted the D and G ratio of the synthesized composite materials.

Table-1: The $I_D$ and $I_G$ ratio of Co-CNTs, Co-lignin and Co-CNTs/lignin as given below.

| S. No. | Materials | $I_D$ | $I_G$ | $I_D/I_G$ |
|---|---|---|---|---|
| 01 | Co-CNTs | 1344 | 1594 | 0.84 |
| 02 | Co-lignin | 1339 | 1601 | 0.83 |
| 03 | Co-CNTs/lignin | 1352 | 1597 | 0.85 |

X-ray photoelectron spectroscopy was utilized to investigate the surface composition and chemical states of the Co-CNTs/lignin composite. The survey spectrum, shown in Fig. 3(c-g), confirms the presence of carbon, oxygen, nitrogen, and cobalt indicating a complex surface composition consisting of these elements. Detailed analysis of the high-resolution spectra for Co 2p, C 1s, N 1s, and O 1s provided insights into the chemical bonding and oxidation states. the Co 2p spectrum (Fig. 3(d)) shows two distinct peaks at approximately 783.11 eV and 796.29 eV, corresponding to Co $2p_{3/2}$ and Co $2p_{1/2}$, respectively. These peaks, when further resolved, reveal spin–orbit components indicative of both $Co^{2+}$ and $Co^{3+}$ oxidation states, as previously reported [33]. $Co2p_{3/2}$ and Co $2p_{1/2}$ can be further split into two spin–orbit lines, evidencing the presence of divalent and trivalent Co species [34]. The high-resolution O1 spectrum (Fig. 3(e))) can be de composed into three peaks corresponding to Co–OH (524.53 eV), Co–O–C (530.68 eV), and Co–O (537.25 eV), respectively. One of them at the binding energy of 530.68 eV corresponds to the Co–O–C bond of the oxygen-containing functional group on the surface of CNTs [35]. As shown in Fig. 3(f), the high-resolution N 1s spectra visualize the presence of four forms of N species for all of the synthesize sample, namely, pyridinic N (397.84 eV, N-6), pyrrolic/pyridine N (400.67 eV, N-5), graphitic N (402.69 eV, N-Q), and pyridine N-oxide (403.88 eV, N-X), which are mainly obtained by carbonization of nitrogen-containing precursor [36]. As shown in the C 1s spectrum (**Fig. 3**(g)), the XPS C 1s spectrum exhibits two peaks: one at 288.77eV corresponding to C=C/C–C bonds and another at 286.97 eV, associated with C–O bonds [34].

The porosity also plays an important role in the electrochemical performance of cobalt-doped carbon nanotubes lignin, as well as the morphology. The porosity of the Co-CNTs/lignin was characterized by nitrogen adsorption−desorption isotherms to understand the effect of CNTs growth on the specific surface area and pore structure of materials, as shown in Fig 3(h). The materials have very type IV isotherm with a hysteresis loop (Fig 3a), which suggests the presence of abundant mesoporosity in the synthesized Co-CNTS/lignin sample. The calculated BET surface area of Co-CNTs/lignin is 703.6 $m^2\ g^{-1}$, but the pore size distribution of of the sample presented inset (Fig), and the pore size is concentrated at 1.6 and 3.5 nm. It is clear that after the growth of CNTs, the pore volume of the material is (0.39 $cm^3\ g^{-1}$). The good conductivity and the 3D network of dendritic CNTs on the Co-lignin, which could enhance the electrochemical performance of the synthesized sample. Fig. 3(i) presents the thermal behavior of the synthesized Co-CNTs/lignin nanocomposite material. Thermogravimetric analysis was conducted in an air atmosphere with a heating rate of 10 °C $min^{-1}$. As verified by the thermogravimetric analysis, the mass contents of Co-element in Co-CNTs/lignin nanocomposite are 26.96 wt%.

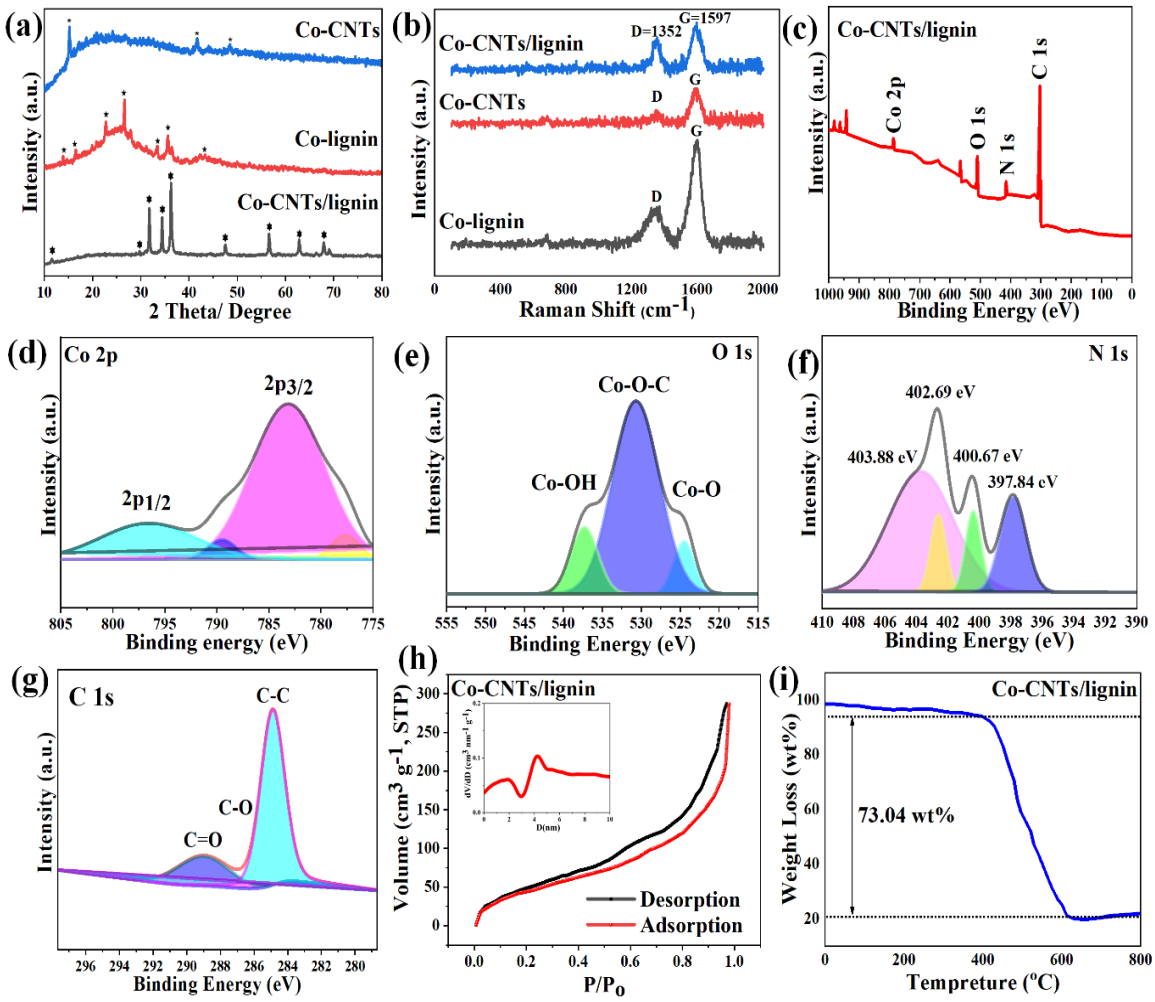


Fig. 3: (a) XRD patterns of the composite and pristine samples that confirm the formation of a crystalline structure, (b) Raman spectra of the all samples, (c) XPS spectra, high-resolution XPS spectra of Co-CNTs/lignin, (d) Co 2p, (e) O 1s, (f) N 1s , (g) C 1s XPS survey spectra, (h) $N_2$ adsorption-desorption isotherms and the pore size distribution curves of the fabricated Co-CNTs/lignin particles, and (i) Thermogravimetric analysis of Co-CNTs/lignin.

*Electrochemical Measurements*

Cyclic voltammetry was used to examined the electrochemical characteristics of the synthesized composite materials. The measurements was performed at different scan rates, ranging from 2 mV $s^{-1}$ to 200 mV $s^{-1}$, as shown in Fig. 4(a-c). The materials at a scan rate of 2 mV $s^{-1}$, as shown in Fig. 4(d), it is evident that the Co-CNTs/lignin-GCE composite has a much greater response in comparison to the other two synthesized materials. The CV curves display well-defined redox peaks, indicating that the developed carbon materials possess excellent pseudo-capacitance behaviour. This enhances the efficacy of ion transportation and assimilation. The composite samples CV curves showed notable variations in capacitance performance among different loop portions. This study showed that the addition of CNTs had a substantial effect on the electrochemical performance of the nanocomposite material, resulting in improved characteristics. The Co-CNTs/lignin sample exhibited a significantly greater surface area compared to the other Co-CNTs and Co-lignin samples, as shown in Fig. 4(d). The existence of two peaks in the current density signifies the occurrence of a faradaic reaction, which is an electrochemical reaction involving the transfer of a substantial quantity of electrons and ions. This suggests that the reaction is

a complex process that involves multiple species and possibly multiple electron transfer steps [37]. The faradaic reaction encompasses two sets of redox reactions ( oxidation & reduction), which are described by the following equations [38, 39]:

$$Co + 2OH \rightarrow Co(OH)_2 + 2e^- \quad (4)$$

$$2Co(HO)_2 + 2HO + e^- \rightarrow Co_2O_3 + 3H_2O + 2e^- \quad (5)$$

The electrode material exceptional pseudo-capacitance is due to the faradaic processes, which are further intensified by the extremely concentrated electrolyte of 6 M KOH. This concentrated electrolyte provides a surplus of hydroxide ions ($HO^-$), facilitating the faradaic reactions and resulting in exceptional capacitive performance. The observed change in oxidation and reduction peaks in the CV curves as the scan rate increases suggests that the faradaic processes are governed by diffusion. In other words, the rate at which ions diffuse controls the reaction kinetics [40]. This implies that the movement of ions towards the electrode surface takes time, and in addition, the chemical reaction happening on the surface of the large Co particles is also influenced by time. Consequently, when the voltage fluctuates quickly, the ideal voltage for the faradaic processes gradually moves, causing a delay between the voltage change and the corresponding faradaic response. This delay is due to the limited time needed for ionic diffusion and reaction kinetics [41]. Furthermore, the capacitance curves of the three synthesized samples at different scan rates clearly show that Co-CNTs/lignin performs better than the other two synthesized materials, as shown in Fig. 4(e). This superior response underscores the exceptional electrochemical properties of Co-CNTs/lignin, as compare to pristine samples. Fig. 4(f) illustrates the peak current densities for the oxidation and reduction of the synthesized ocomposite material Co-CNTs/lignin as a function of scan rate.

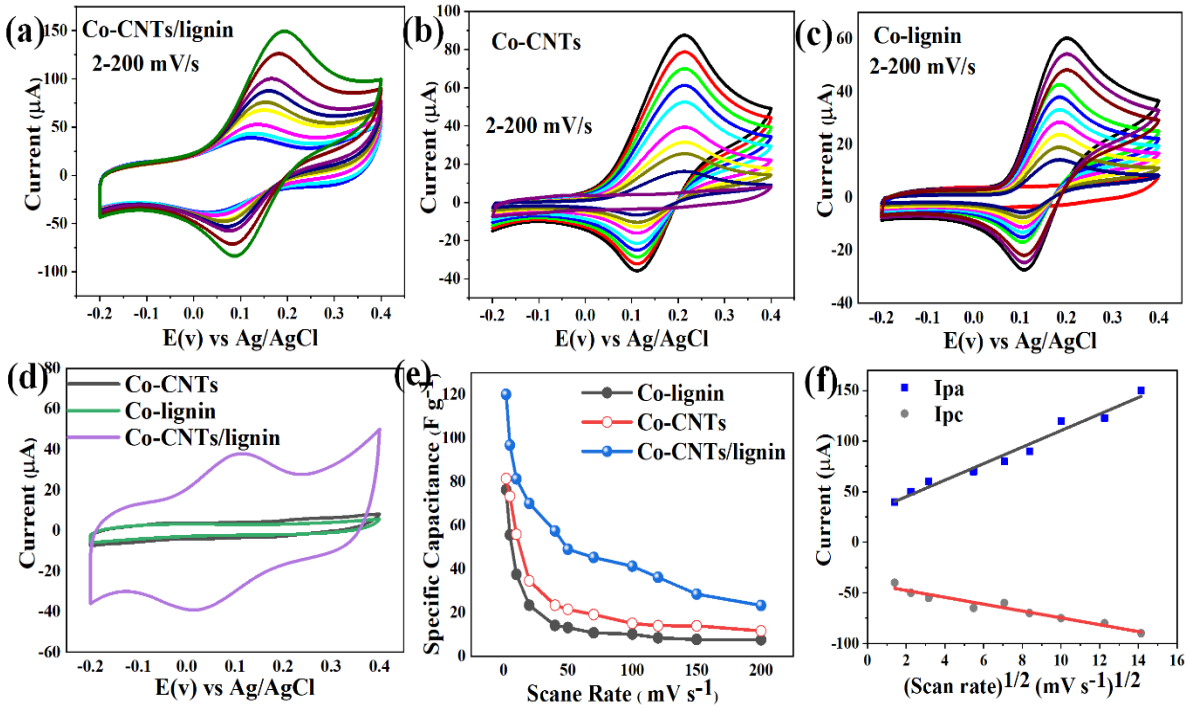


Fig. 4: (a-c) Cyclic Voltammograms of the synthesized all samples at different scan rates, (c) Comparison of cyclic voltammograms of the all samples at a constant scan rate of 2 mV $s^{-1}$, (d) Capacitance curves of the samples at different scan rates, and (e) oxidation and reduction of the composite Co-CNTs/lignin peak current densities as a function of scan rate.

Electrochemical impedance spectroscopy is a powerful analytical technique used to investigate the electrochemical properties of various electrode materials, and understanding the performance and potential applications of electrode materials in energy storage and conversion devices [42, 43]. The EIS was used to characterize the synthesized Co-CNTs, Co-lignin and Co-CNT/lignin electrodes materials, and the Nyquist plots the all three samples, as shown in Fig. 5 (a). The objective was to comprehend the mechanism by which the contact between the liquid electrodes enhances the conduction of electricity and charges. The EIS experiments employed a direct current (DC) bias of 1.75, encompassing frequencies ranging from 0.1 to $10^5$ kilohertz and the randles circuit (RC) is used to adjust the Nyquist plot, as inset in Fig. 5 (a). Electrons exhibit enhanced migration and faster response rates. All of the synthetic samples exhibited a pattern that was characterized by both curvature and modest linearity, which is typical of capacitors. This is due to the abundance of mesopores and macropores present in synthetic materials. Currently, the samples have a clearly delineated semi-circular shape. The magnitude of the charge transfer resistance at the interface between the electrode and electrolyte is directly proportional to the size of the semicircular arc. The resistance is determined by the impedance of electron transport at the electrode-liquid interface. The width of the semicircle might be used as an indicator of its size [44]. The series resistance values of 59.46 Ω, 60.98 Ω, and 61.41 Ω when used with Co-CNTs, Co-lignin, and Co-CNTs/lignin, respectively. The charge transfer resistance for Co-CNTs, Co-lignin and Co-CNTs/lignin are 18.23 Ω, 24.39 Ω, and 14.04 Ω, respectively. The Co-CNTs/lignin composite exhibits a remarkable suite of properties, rendering it an attractive candidate for electrode applications. Notably, it displays a high specific capacitance, signifying its capacity to store substantial electrical charge, exceptional energy density, highlighting its potential for energy storage and related uses, and low impedance, indicative of efficient electron transfer kinetics and rapid charge/discharge rates.

To determine the material's electrochemical characteristics, galvanostatic charge-discharge experiments was performed in a 6M KOH electrolyte at current densities of 0.5, 1 and 2 A $g^{-1}$, respectively, as shown in **Fig. 5**(b). Equations (1), (2), and (3) was used to calculate specific capacitance, energy density, and power density. This information provides important insights about the material's ability to store and release energy, as well as its potential usage in energy storage systems. The GCD curves displayed triangular shapes with a regular pattern, which suggests that the material behaves like an electric double-layer energy storage device. Furthermore, the GCD curves showed symmetrical triangular shapes, indicating that the material could swiftly change both direction and velocity. This feature makes it ideal for applications needing high-performance energy storage [45]. The Co-CNTs/lignin composite material had excellent electrochemical performance, with a specific capacitance of 1977.9 F $g^{-1}$, an energy density of 98.9 Wh $kg^{-1}$, and a power density of 450.02 W $kg^{-1}$ at a low current density of 0.5 A $g^{-1}$. However, raising the current density to 2 A $g^{-1}$ resulted in a significant reduction in performance measurements. Specifically, the specific capacitance decreased to 1235.1 F $g^{-1}$, the energy density to 61.76 Wh $kg^{-1}$, and the power density to 191.32 W$kg^{-1}$. This indicates that while the material exhibits outstanding performance at low current densities, its performance diminishes as the current density increases. This reduction in performance is attributed to the shortened diffusion time for ions to penetrate the electrode material and the incomplete redox reaction due to the higher current density [40]. The composite material remarkable electrochemical performance ascribed primarily to its huge specific surface area and well-structured porosity. This intricate structure, comprising numerous micropores and mesopores, facilitates efficient mass transport and reaction kinetics, thereby contributing to the material's outstanding capabilities in energy storage and conversion applications. The mesopores enhance electrolyte conductivity and facilitate rapid ion transport, leading to exceptional rate capability. The existence of micropores increases the specific surface area and pore volume, allowing for active charge storage and resulting in a significant increase in capacitance [46]. Fig. 5(c) displays the composite material specific capacitance at various current densities.

The cyclic performance of Co-CNTs/lignin composite electrode material in the three-electrode system, illustrated in Fig. 5(d), exhibits outstanding stability. At a current density of 5 A $g^{-1}$, the electrode retained 98% of its initial capacity after 1000 charge-discharge cycles. This demonstrates that it has excellent cycling performance and very minimal capacity decay. The high columbic efficiency of 81% remained consistent throughout the cycles, indicating a highly reversible system. Furthermore, the negligible changes in columbic and energy efficiencies after 1000 cycles underscore the system’s reversibility and robustness.

A comparative analysis presented in Table 2 reveals that our energy storage performance is comparable to, or in some cases, exceeds that of recently reported composite nanomaterials. While our specific capacitance demonstrates superior results, there remains opportunity for further optimization to enhance the energy storage capabilities of Co-CNTs/lignin. This finding motivates continued refinement of our material to achieve even greater performance enhancements.

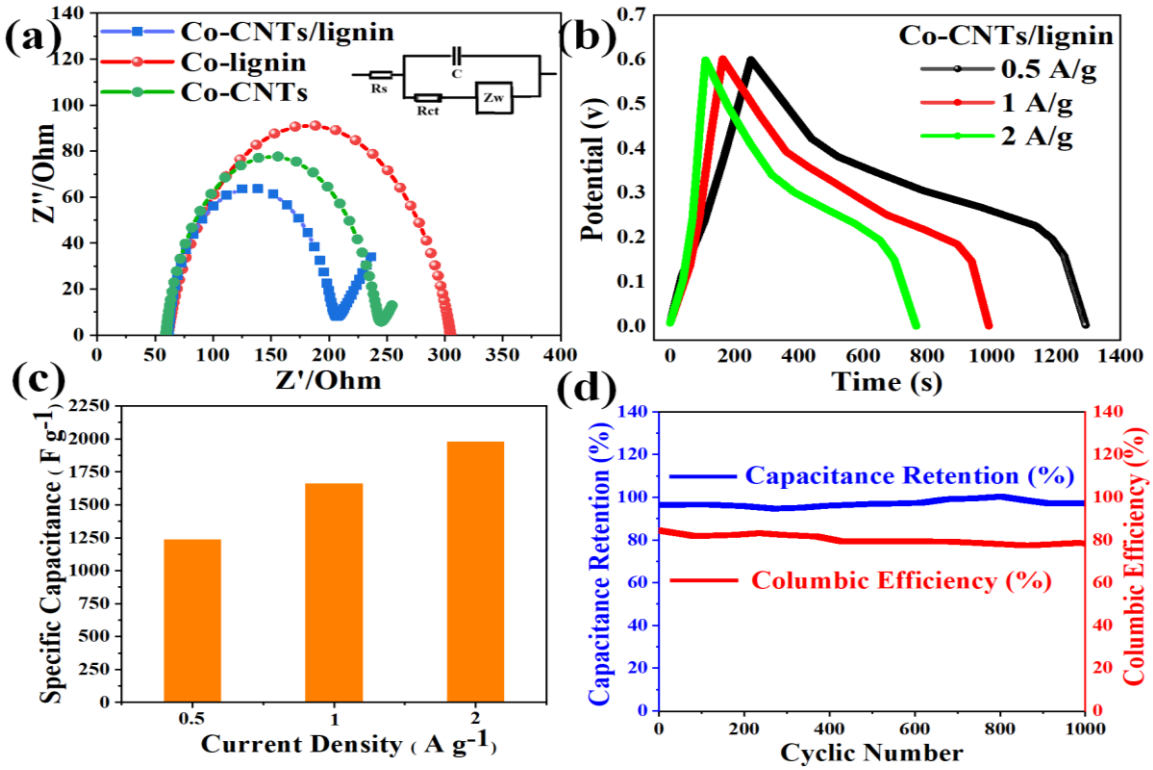


Fig. 5: (a) EIS Nyquist plot analysis of the all sample in the frequency range of 0.1 to $10^5$ KHz and inset equivalent circuit to adjust the Nyquist plot, (b) GCD curves of synthesized Co-CNTs/lignin at different current densities with a potential range of 0.0 to 0.6V, (b) specific capacitance at different current density, and (d) cyclic performance of the Co-CNTs/lignin composite at the current density of 5 A $g^{-1}$

Table-2: Comparative analysis of various energy storage materials and our synthesized composite along with their performance.

| S. No. | Materials | Electrolytes | Current density (A $g^{-1}$) | Specific capacitance (F $g^{-1}$) | Energy density (Wh $kg^{-1}$) | Power density (W $kg^{-1}$) | Ref. |
|---|---|---|---|---|---|---|---|
| 01 | Ni@CNTs@$Co_9S_8$ | 3 M KOH | 1 | 1305.4 | 23.8 | 8007.4 | [47] |
| 02 | rGO/PANI/PVA-$H_2SO_4$/AC | 1 M $H_2SO_4$ | -- | 1348 | 20 | -- | [48] |
| 03 | NiCoLDH@LHE | 2 M KOH | 1 | 640 | 35.44 | 200.1 | [49] |
| 04 | LC30 | 6 M KOH | 0.5 | 216.2 | 12.3 | 50 | [20] |
| 05 | Co-NCNT | 0.1 M KOH | -- | -- | -- | 130 | [50] |
| 06 | WCS10 | 2 M KOH | 6 | 1720 | -- | -- | [51] |
| 07 | AILCFN/Ni-Co-S | 6 M KOH | 10 | 1040 | 30.8 | 800 | [52] |
| 08 | Cu-CNTs/lignin | $H_2SO_4$ | 0.5 | 963.75 | 48.18 | 150 | [53] |
| 09 | Co-CNTs/ligin | 6 M KOH | 0.5 | 1977.9 | 98.9 | 450.02 | Present Work |

## Conclusion

In summary, we successfully synthesized Co-CNTs/lignin composite material incorporating CNTs and cobalt with lignin matrix via a hydrothermal process. These composite material exhibited markedly enhanced electrochemical performance over then pristine sample [Co-CNTs, Co-lignin] with enhanced discharge capacities and superior cycle stability. The optimized nanocomposite electrode, designated as Co-CNTs/lignin-GCE, showcased very high specific capacitance (1977.9 F $g^{-1}$), power density (450.02 W $kg^{-1}$) and an energy density (98.9 Wh $kg^{-1}$) at the current density of 0.5 A $g^{-1}$. Additionally, after 1000 charge-discharge cycles at current density of 5 A $g^{-1}$, the composite material demonstrated 98% of its capacitance retention, and exhibited remarkable coulombic efficiency of 81%. This enhance performance is attributed to the effects of CNTs and lignin, which prevent the agglomeration of nanoparticles and preserve the structural integrity during cycling. Our findings indicate that the

incorporation of CNTs into lignin significantly increases its capacity and cycle stability. The findings reveal that the electrode material composed of components functions very well, making it an excellent alternative for energy storage devices. To further enhance the performance and practical applicability of Co-CNTs/lignin composites, future research should focus on several key areas. To optimizing the ratio and dispersion of Co nanoparticles and CNTs within the lignin matrix could further improve electrochemical stability and capacity. Also exploring the influence of different lignin sources and functionalization strategies may unlock tunable electrochemical behavior and structural properties. Additionally, integrating the composite into full-cell configurations and testing under realistic operating conditions (e.g., flexible or wearable devices) would validate its feasibility for real-world energy storage applications.

**References**


1. H. Liu, T. Xu, K. Liu, M. Zhang, W. Liu, H. Li, C. Si, Lignin-based electrodes for energy storage application. *Industrial Crops and Products*, ***165***, 113425 (2021).
2. L. Hu, W. Chen, X. Xie, N. Liu, Y. Yang, H. Wu, Y. Cui, Symmetrical MnO2–carbon nanotube–textile nanostructures for wearable pseudocapacitors with high mass loading. *ACS nano*, ***5***(11), 8904-8913 (2011).
3. H. Huang, & X. Wang, Graphene nanoplate-MnO 2 composites for supercapacitors: a controllable oxidation approach. *Nanoscale*, ***3***(8), 3185-3191 (2011).
4. E. Raymundo-Pinero, V. Khomenko, E. Frackowiak, & F. Beguin, Performance of manganese oxide/CNTs composites as electrode materials for electrochemical capacitors. *Journal of The Electrochemical Society*, ***152***(1), A229 (2004).
5. H. Wang, H. S. Casalongue, Y. Liang, & H. Dai, Ni (OH) 2 nanoplates grown on graphene as advanced electrochemical pseudocapacitor materials. *Journal of the American Chemical Society*, ***132***(21), 7472-7477 (2010).
6. K. R. Prasad, & N. Miura, Potentiodynamically deposited nanostructured manganese dioxide as electrode material for electrochemical redox supercapacitors. *Journal of power sources*, ***135***(1-2), 354-360 (2004).
7. G. M. Ilari, N. Kränzlin, R. Longtin, J. R. Sanchez-Valencia, S. Schneider, M. D. Rossell, R. Erni, Single-step functionalization of vertically aligned MWCNTs with Cu and Ni by chemical reduction of copper and nickel acetyl acetonate in benzyl alcohol. *Carbon*, ***73***, 146-154 (2014).
8. A. Bengtsson, J. Bengtsson, M. Sedin, & E. Sjöholm, Carbon fibers from lignin-cellulose precursors: effect of stabilization conditions. *ACS Sustainable Chemistry & Engineering*, ***7***(9), 8440-8448 (2019).
9. R. Xu, C. I Si, F. G. Kong, & X. Y. Li, Synthesis of γ-valerolactone and its application in biomass conversion (2020).
10. Z. U. Khan, J. Jiang, & M. Y. A. Khan, A comprehensive review on recent advancements in new carbon and metal-organic framework base energy storage materials and devices. *Journal of Energy Storage*, ***100***, 113464 (2024).
11. J. H Choi, S. K Jang, J. H. Kim, S. Y. Park, J. C. Kim, H. Jeong, H., Choi, I.-G. (2019). Simultaneous production of glucose, furfural, and ethanol organosolv lignin for total utilization of high recalcitrant biomass by organosolv pretreatment. *Renewable Energy*, ***130***, 952-960.
12. S. Admassie, F. Ajjan, A. Elfwing, & O. Inganäs, Biopolymer hybrid electrodes for scalable electricity storage. *Materials Horizons*, ***3***(3), 174-185 (2016).
13. L. Dai, Q. Cao, K. Wang, S. Han, C. Si, D. Liu, & Y. Liu, High efficient recovery of L-lactide with lignin-based filler by thermal degradation. *Industrial Crops and Products*, ***143***, 111954 (2020).
14. L. Tao, A. Hu, Z. Yang, Z. Xu, C. E. Wall, A. R. Esker, F. Lin, A surface chemistry approach to tailoring the hydrophilicity and lithiophilicity of carbon films for hosting high-performance lithium metal anodes. *Advanced Functional Materials*, ***30***(31), 2000585 (2020).
15. Y. Li, D. Cui, Y. Tong, & L. Xu, Study on structure and thermal stability properties of lignin during thermostabilization and carbonization. *International journal of biological macromolecules*, ***62***, 663-669 (2013).
16. X. You, J. Duan, K. Koda, T. Yamada, & Y. Uraki, Preparation of electric double layer capacitors (EDLCs) from two types of electrospun lignin fibers. *Holzforschung*, ***70***(7), 661-671 (2016).
17. H. Jia, N. Sun, M. Dirican, Y. Li, C. Chen, P. Zhu, .J. Tao, Electrospun kraft lignin/cellulose acetate-derived nanocarbon network as an anode for high-performance sodium-ion batteries. *ACS Applied Materials & Interfaces*, ***10***(51), 44368-44375 (2018).
18. J. H. Park, H. H. Rana, J. Y. Lee, & H. S. Park, Renewable flexible supercapacitors based on all-lignin-based hydrogel electrolytes and nanofiber

electrodes. *Journal of Materials Chemistry A*, ***7***(28), 16962-16968 (2019).
19. S. W. Pattinson, K. Prehn, I. A. Kinloch, D. Eder, K. K. Koziol, K. Schulte, & A. H. Windle, The life and death of carbon nanotubes. *RSC advances*, ***2***(7), 2909-2913 (2012).
20. Y. Lin, C. Huang, C. Huang, Y. Deng, X. Zou, W. Ma, A. J. Ragauskas, Cellulose regulated lignin/cellulose-based carbon materials with hierarchical porous structure for energy storage. *Advanced Composites and Hybrid Materials*, ***7***(2), 51 (2024).
21. M. Kim, D. H. Nam, H. Y. Park, C. Kwon, K. Eom, S. Yoo, H. Kwon, Cobalt-carbon nanofibers as an efficient support-free catalyst for oxygen reduction reaction with a systematic study of active site formation. *Journal of Materials Chemistry A*, ***3***(27), 14284-14290. (2015).
22. C. Y. Lu, & M. Y. Wey, The performance of CNT as catalyst support on CO oxidation at low temperature. *Fuel*, ***86***(7-8), 1153-1161 (2007).
23. G. Dresselhaus, M. S. Dresselhaus, & R. Saito, *Physical properties of carbon nanotubes*: *World scientific*. (1998).
24. M. Neelakantan, S. Marriappan, J. Dharmaraja, T. Jeyakumar, & K. Muthukumaran, Spectral, XRD, SEM and biological activities of transition metal complexes of polydentate ligands containing thiazole moiety. *Spectrochimica Acta Part A: Molecular and Biomolecular Spectroscopy*, ***71***(2), 628-635 (2008).
25. M. Molamohammadi, A. Arman, A. Achour, B. Astinchap, A. Ahmadpourian, A. Boochani, A. Ahmadpourian, Microstructure and optical properties of cobalt–carbon nanocomposites prepared by RF-sputtering. *Journal of Materials Science: Materials in Electronics*, ***26,*** 5964-5969 (2015).
26. A. C. Dillon, M. J. Heben, T. Gennett, T., & P. A. Parilla, Metal-doped single-walled carbon nanotubes and production thereof: Google Patents. (2007).
27. R. Shu, Y. Wu, X. Li, N. Li, & J. Shi, Fabrication of bimetallic metal–organic frameworks derived cobalt iron alloy@ carbon–carbon nanotubes composites as ultrathin and high-efficiency microwave absorbers. *Journal of Colloid and Interface Science*, ***613***, 477-487 (2022).
28. J. C. Espinosa, P. Manickam-Periyaraman, F. Bernat-Quesada, S. Sivanesan, M. Álvaro, H. García, & S. Navalón, Engineering of activated carbon surface to enhance the catalytic activity of supported cobalt oxide nanoparticles in peroxymonosulfate activation. *Applied Catalysis B: Environmental*, ***249***, 42-53 (2019).
29. S. Karimi, A. Tavasoli, Y. Mortazavi, & A. Karimi, Cobalt supported on Graphene–A promising novel Fischer–Tropsch synthesis catalyst. *Applied Catalysis A: General*, ***499***, 188-196 (2015).
30. H. Zhang, C. Lancelot, W. Chu, J. Hong, A. Y. Khodakov, P. A. Chernavskii, .D. Tong, The nature of cobalt species in carbon nanotubes and their catalytic performance in Fischer–Tropsch reaction. *Journal of Materials Chemistry*, ***19***(48), 9241-9249 (2009).
31. R. Mehdi, S. R. Naqvi, A. H. Khoja, & R. Hussain, Biomass derived activated carbon by chemical surface modification as a source of clean energy for supercapacitor application, *Fuel*, ***348***, 128529 (2023).
32. L. Torrente-Murciano, A. K. Hill, & T. E. Bell, Ammonia decomposition over cobalt/carbon catalysts—Effect of carbon support and electron donating promoter on activity. *Catalysis Today*, ***286***, 131-140 (2017).
33. I. Shown, A. Ganguly, L. C. Chen, & K. H. Chen, Conducting polymer-based flexible supercapacitor. *Energy Science & Engineering*, ***3***(1), 2-26 (2015).
34. Z. Lv, Y. Luo, Y. Tang, J. Wei, Z. Zhu, X. Zhou, & X. Chen, Editable supercapacitors with customizable stretchability based on mechanically strengthened ultralong MnO2 nanowire composite. *Advanced Materials*, **30**(2), 1704531, (2018).
35. B. Wan, J. Guo, W. H. Lai, Y. X. Wang, M. Liu, H. K. Liu, & S. X. Dou, Layered mesoporous CoO/reduced graphene oxide with strong interfacial coupling as a high-performance anode for lithium-ion batteries. *Journal of Alloys and Compounds*, ***843***, 156050, (2020).
36. X. F. Li, K. Y. Lian, L. Liu, Y. Wu, Q. Qiu, J. Jiang, ... & Y. Luo, Unraveling the formation mechanism of graphitic nitrogen-doping in thermally treated graphene with ammonia. *Scientific Reports*, ***6***(1), 23495, (2016).
37. S. Hu, E. L. Ribeiro, S. A. Davari, M. Tian, D. Mukherjee, & B. Khomami, Hybrid nanocomposites of nanostructured Co 3 O 4 interfaced with reduced/nitrogen-doped graphene oxides for selective improvements in electrocatalytic and/or supercapacitive properties. *RSC advances*, ***7***(53), 33166-33176 (2017).
38. K. M. Ismail, & W. Badawy, Electrochemical and XPS investigations of cobalt in KOH solutions. *Journal of applied electrochemistry*, ***30***, 1303-1311 (2000).
39. R. Cowling, & A. Riddiford, A. The anodic behaviour of cobalt in alkaline solutions. *Electrochimica Acta*, ***14***(10), 981-989 (1969).

40. A. C. Forse, J. M. Griffin, C. Merlet, J. Carretero-Gonzalez, A. R. O. Raji, N. M. Trease, & C. P. Grey, Direct observation of ion dynamics in supercapacitor electrodes using in situ diffusion NMR spectroscopy. *Nature Energy*, ***2***(3), 1-7 (2017).
41. H. Wu, D. He, & Y. Wang, Electrode materials of Cobalt@ Nitrogen doped carbon nano rod/reduced graphene oxide on Nickel foam by electrophoretic deposition and 3D rGO aerogel for a high-performance asymmetrical supercapacitor. *Electrochimica Acta*, ***343***, 136117 (2020).
42. Y. Yan, P. Gu, S. Zheng, M. Zheng, H. Pang, & H. Xue, Facile synthesis of an accordion-like Ni-MOF superstructure for high-performance flexible supercapacitors. *Journal of Materials Chemistry A*, ***4***(48), 19078-19085 (2016).
43. J. N. Lekitima, K. I. Ozoemena, C. J. Jafta, N. Kobayashi, Y. Song, D. Tong, M. Oyama, M, High-performance aqueous asymmetric electrochemical capacitors based on graphene oxide/cobalt (ii)-tetrapyrazinoporphyrazine hybrids. *Journal of Materials Chemistry A*, ***1***(8), 2821-2826, (2013).
44. H. Yang, M. Sang, G. Li, D. Zuo, J. Xu, & H. Zhang, Stretchable, self-healable, conductive and adhesive gel polymer electrolytes based on a deep eutectic solvent for all-climate flexible electrical double-layer capacitors. *Journal of Energy Storage*, ***45***, 103766 (2022).
45. Y. Zhao, P. Chen, S. Tao, X. Zu, S. Li, & L. Qiao, Nitrogen/oxygen co-doped carbon nanofoam derived from bamboo fungi for high-performance supercapacitors. *Journal of power sources*, ***479***, 228835. (2020).
46. C. Li, X. Zhang, Z. Lv, K. Wang, X. Sun, X. Chen, & Y. Ma, Scalable combustion synthesis of graphene-welded activated carbon for high-performance supercapacitors. *Chemical Engineering Journal*, ***414***, 128781 (2021).
47. S. Zeng, X. Wang, Y. Zhang, J. Shao, Z. Ding, & J. Zhao, Uniform Co9S8 nanosheets on carbon nanotube arrays grown on Ni mesh as free-standing electrodes for asymmetric supercapacitors. *Diamond and Related Materials*, ***141***, 110570 (2024).
48. D. Pawar, D. Malavekar, A. Lokhande, & C. Lokhande, Facile synthesis of layered reduced graphene oxide/polyaniline (rGO/PANI) composite electrode for flexible asymmetric solid-state supercapacitor. *Journal of Energy Storage*, ***79,*** 110154 (2024).
49. M. Liu, B. Farhadi, W. Li, L. An, Y. Li, Z. Zou, K. Wang, Nickel-cobalt layer double hydroxide@ lignin-based hollow carbon quasi core-shell structure for high-performance supercapacitors. *Electrochimica Acta*, ***478***, 143836 (2024).
50. Q. Liao, G. Li, R. Ding, Z. He, M. Jiang, C. Zhao, H. He, Facile synthesis of CO/N-doped carbon nanotubes and the application in alkaline and neutral metal-air batteries. *International Journal of Hydrogen Energy*, ***46***(61), 31253-31261 (2021).
51. M. Murmu, A. T. Sivagurunathan, S. Adhikari, & D. H. Kim, Tailoring the interface in tungsten doped cobalt sulfide positive electrode with ultrathin cobalt oxide atomic layer for high performance energy storage application. *Journal of Energy Storage*, ***91***, 111993 (2024).
52. M. Zhou, A. Bahi, Y. Zhao, L. Lin, F. Ko, P. Servati, Q. Wang, Enhancement of charge transport in interconnected lignin-derived carbon fibrous network for flexible battery-supercapacitor hybrid device. *Chemical Engineering Journal*, ***409***, 128214 (2021).
53. Z. U. Khan, J. Jiang, A. Kusar, M. Y. A. Khan, F. Ali, & A. Zahoor, Fabrication of Copper-Doped Lignin-Based Carbon Nanotube Composite Electrodes for Energy Storage Applications. In 2024 21st International Bhurban Conference on Applied Sciences and Technology (IBCAST), 118-122. IEEE. (2024).